
**STRENGTH
AND PLASTICITY**

Effect of the Repetitive Corrugation and Straightening on the Microstructure and Mechanical Properties of a 3003 Aluminum Alloy

C. Reyes-Ruiz^{a,*}, C. G. Figueroa^b, G. González^c, and A. Ortiz^a

^a *Departamento de Diseño y Manufactura, Facultad de Ingeniería, Universidad Nacional Autónoma de México,
Cd. Universitaria, Mexico, 04510 Mexico*

^b *Departamento de Diseño y Manufactura, Facultad de Ingeniería, Universidad Nacional Autónoma de México, PIIT,
Apodaca, 66629 Mexico*

^c *Instituto de Investigaciones en Materiales, Universidad Nacional Autónoma de México,
Cd. Universitaria, Mexico, 04510 Mexico*

**e-mail: c.reyesruiz@unam.com*

Received October 27, 2020; revised January 11, 2021; accepted January 19, 2021

Abstract—A novel repetitive corrugation and straightening (RCS) die geometry was evaluated in terms of its mechanical properties and microstructural modifications. An annealed 3003 aluminum alloy sheet was processed up to 6 RCS passes at room temperature, showing a significant improvement in yield strength and hardness. Changes in surface profile values were obtained along different stages of the repetitive process; this showed a clear correlation between the higher strained region and the maxima of hardness values. Moreover, differences in roughness were associated with real contact area between material and corrugating die sections. Local strain distribution generated during the process was determined by kernel average misorientation (KAM) and was consistent with microhardness mapping results. Orientation image mapping showed that grains, with the normals parallel to $\langle 111 \rangle$, activate dislocation arrangement and grain fragmentation process prior to other main directions. In spite of mechanical properties improvement, initial texture components were maintained.

Keywords: repetitive corrugated and straightening, AA3003, severe plastic deformation, microhardness, texture, EBSD

DOI: 10.1134/S0031918X21050112

INTRODUCTION

Severe plastic deformation (SPD) techniques have been widely investigated recently due to their capability of improving the yield strength, hardness, and fatigue resistance, through grain refinement up to ultra-fine grain size. Such changes occur without affecting specimen geometry but by introducing a large amount of dislocations in each pass of a repetitive process [1–3]. Several industrial sectors are interested in the above mentioned properties, in particular, the automotive and aerospace industries that require particularly elevated yield stress on low-density materials, such as aluminum alloys. Among the more cited SPD techniques: Equal channel angular pressing (ECAP) [4–6], high pressure torsion (HPT) [7], multi-axial compression (MAC) [8], constrained groove pressing (CGP) [9], accumulative roll bonding (ARB) [10], repetitive corrugation and straightening (RCS) [11, 12], the last is one of the simplest to perform and is well adapted for improving the mechanical strength of metallic sheets. As a result of the SPD techniques, a

strain up to ~ 10 can be reached, with the grain size diminished considerably [13–15]. Therefore, it is extremely important to follow the grain size and the grain misorientation evolution at highly deformed stages, where dynamic recovery could take place, even at low temperatures [16–18]. As other SPD techniques, RCS process has revealed its ability to produce bulk nanostructured materials [12], several RCS dies have been proposed [19–24], the purpose has been to produce the most homogeneous deformation into the sample, combined with an ultrafine grains microstructure. Recently, it was reported that materials which combine large and small grains at a micrometer scale, could have unexpected mechanical properties [25], such heterogeneous materials could be produced with a new RCS die proposal, promoting heterogeneous strain. Hypothetically, the last could lead to enhanced mechanical properties with not only a mixed UFG microstructure, but also a convenient crystallographic texture which could be suitable for applications. In recent years, RCS reports in alumi-

num alloys focused mainly on the Al–Mg and Al–Li systems. The A3003 alloy has not received attention, despite its corrosion resistance, good formability, and weldability. Furthermore, phenomena produced during friction and in general surface damage, leaving at worn surfaces certain changes in specimen geometry, have been poorly discussed in the literature.

The aim of this study was to evaluate and correlate the mechanical and microstructural effects of a repetitive corrugated and straightening (RCS) process using a novel die geometry, which introduces heterogeneous deformation, in AA3003 alloy. The material was deformed at room temperature by RCS up to six passes. Mechanical properties were characterized by tension tests and microhardness mapping while surface modification was measured by means of an optical profilometer. Crystallographic texture and microstructure changes were investigated through X-ray diffraction peak-broadening, pole figures, and orientation maps obtained by electron backscatter diffraction (EBSD).

EXPERIMENTAL PROCEDURE

Aluminum sheet of 3003 alloy with 1.2 mm thickness was acquired from a commercial distributor under H14 condition of supply. Prior to RCS processing, specimens were annealed at 450°C for 3 h to promote softening. Chemical composition was obtained by means of fluorescence equipment and is presented in Table 1.

RCS process was performed within dies, as is shown in Fig. 1a, on a 112 × 112 mm sheet. Die geometry design was based on a sinusoidal function with an amplitude of 4 mm and a period of 16 mm. First corrugation was applied at a rate of to 5 mm/min. Afterward, the first straighten was induced to the material, marks in Fig. 1b represent lower position of the bottom die. After a 90° rotation, a second corrugation and straightening were achieved, producing new marks shown in Fig. 1c. This double corrugation and straightening process, illustrated in Figs. 1b–1d, is considered as a complete RCS pass, which according to Rosochowski [26], produces an equivalent plastic strain of ~1.1. Considering the die symmetry, dashed area in Fig. 1e indicates location of representative microhardness and grain orientation mapping. During the complete process, MoS₂ was used as lubricant between samples and corrugating and straightening dies. The reference sample is denoted as 0P, while one pass and six passes samples are designated as 1P and 6P, respectively.

Tensile samples were obtained from 0P and deformed samples, all parallel to rolling direction. The tensile tests were carried out at 10⁻³ s⁻¹, using an Instron universal testing machine.

Surface profiles measurement and hardness tests were conducted by means of a Nanovea platform equipped with a chromatic confocal optical profi-

Table 1. Chemical composition of 3003 aluminum alloy

Si	Fe	Cu	Mn	Zn	Others	Al
0.6	0.58	0.1	0.85	0.05	0.1	Balance

meter and a Vickers pyramidal indenter. Microhardness mapping was carried out applying a 1 N load with stabilization time at maximum load of 10 s. A 500 μm step mesh was generated in representative sections previously prepared by mechanical polishing. Considering symmetrical deformation, representative sections were selected as is shown in Fig. 1e. To characterize the surface modification produced by SPD process, height measurements were conducted using an optical profilometer. Processing data consisted in pulling apart shape and roughness by means of fitting to a fifth-degree polynomial. Root mean square roughness (Rrms) was calculated from 1 mm lines placed randomly over processed surfaces in which three different zones were identified, each one corresponding to specific zones in the die contact surface. Mentioned zones are: baseline, deepest zones, and highest zones.

A Rigaku Ultima IV diffractometer equipped with Cu Kα radiation and crossbeam optics (CBO), was used to obtain X-ray diffractograms and crystallographic texture. Pole figures measurements were obtained under “in-plane” mode having a ranging scan α and β of 0°–90° and 0°–360°, respectively. Texture analysis was carried out through orientation distribution function (ODF) calculated by the MATLAB toolbox, MTEX [27].

Under a Bragg–Brentano condition, X-ray diffractograms with 2θ values from 20°–140°, using a 0.01° step and a speed of 0.2°/min were obtained. X-ray peak broadening was determined by Le Bail refinement method within FULLPROF software [28]. LaB₆ standard powder was used to calculate the instrumental peak broadening, deconvoluting the integral breadth from its Gaussian and Lorentzian contributions.

Assuming that X-ray sample profile is mainly Lorentzian, crystallite domain size and strain can be obtained by plotting the Williamson–Hall (W–H) equation which allows to separate crystalline domain size (*D*) and strain (ϵ) contribution from the integral breadth (β), as: $\beta \cos \theta = k\lambda/D + 2\epsilon \sin \theta$ this provides valuable-qualitative information about strain variation as a function of RCS passes.

Electron backscattered diffraction (ESBD) scans were obtained through a field emission JEOL JEM7600FEG scanning electron microscope (SEM). Samples over normal direction were prepared by conventional mechanical polishing, while orientation maps acquisition was performed in selected zones presented in Fig. 1e. MTEX software analysis was used to process orientation data.

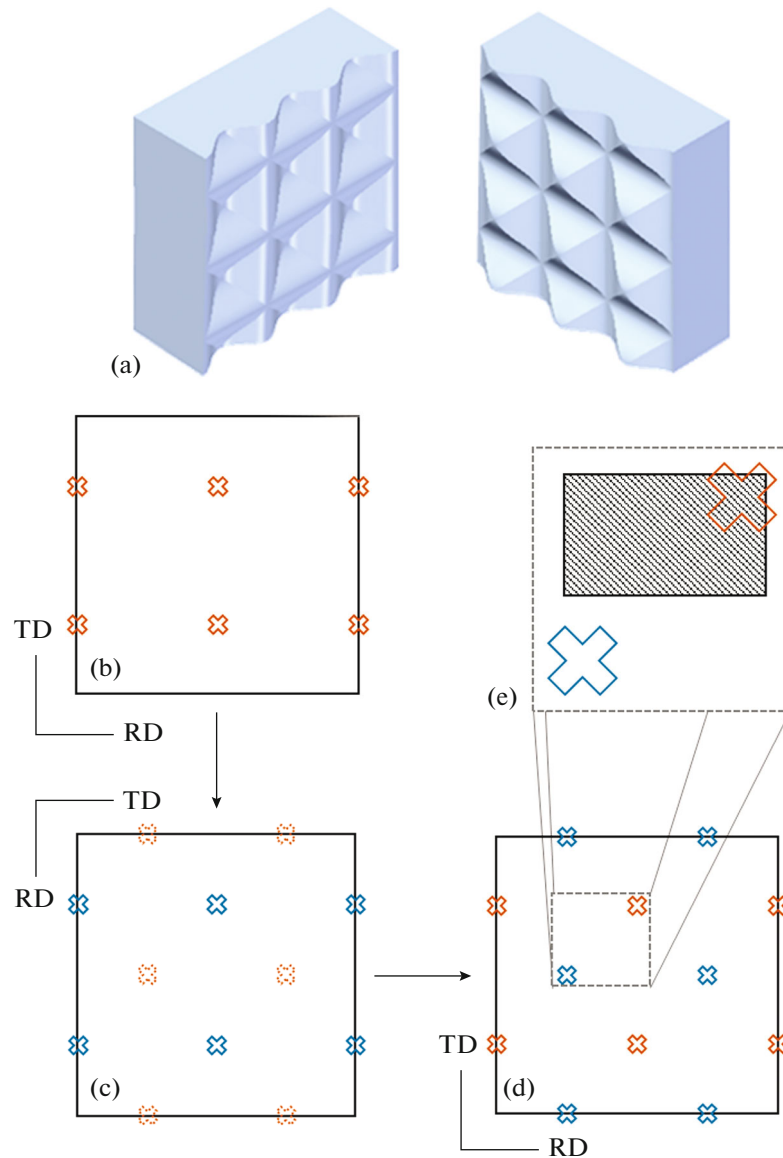


Fig. 1. (a) RCS die geometry. (b), (c), and (d) RCS process scheme. (e) Identification zones for microstructural and mechanical characterization.

RESULTS AND DISCUSSION

RCS process was successfully applied to an annealed 3003 aluminum alloy sheet without visible material damage. The stress-strain curves showed in Fig. 2 present an important increase in yield stress between the 0P and 1P samples. For 0P a yield stress of ~ 57 MPa was obtained while after a complete RCS cycle, ~ 87 MPa was achieved as yield stress value. After six RCS cycles (6P), a marginal increase in yield stress was observed (~ 92 MPa). As a consequence of the increase in yield strength, a reduction in ductility was registered, this is consistent with the observed in the SPD processing conducted at room temperature [29]. Despite this strengthening, nowadays there are other mechanical and microstructural

properties and capabilities that require scrutiny in the SPD field [30].

Microhardness obtained from a representative zone of the 0P sample showed homogeneous hardness values of 31 ± 0.5 HV. Microhardness distribution through deformed 1P and 6P samples, obtained from dashed zone in Fig. 1(e), are shown in Fig. 3. In both samples, the highest hardness values are related to most strained zones which correspond to the hills in the bottom corrugating die. In the 1P sample, the maximum hardness increasing is about 50% from the reference value, while in the case of 6P an additional hardening increase of 10% was registered. Additionally, hardness increment showed a spread that extends over a larger region as the number of passes increases.

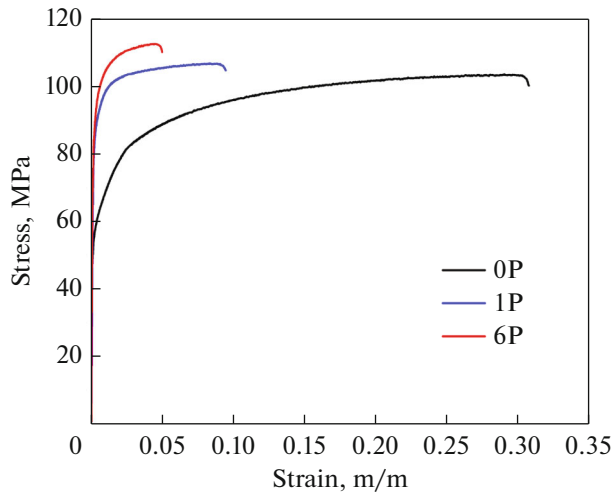


Fig. 2. Stress–strain curves for 0P, 1P, and 6P samples.

These results could be useful depending on the final application due to that a gradient in hardness distribution is desired in some materials like those subjected to sliding contact conditions [31].

Some 3D height profiles for 1P and 6P samples are presented in Figs. 4a, 4d, respectively. It is observed that as the number of passes increases, the morphology of processed material is better defined, due to that the highest and lowest zones are closer to the baseline. This allows to identify each zone as is referred in Figs. 4c, 4e, which show the surface shape data after one and six passes, making evident two zones that do not fulfill the baseline, these are identified as A and B. In the case of zone A, the material is under the baseline due to the induced pileup in surroundings to hardest region, this is according to the roughness map (Figs. 4c, 4f) where it is possible to notice higher roughness values indicating a greater contact area. In zone B, lower height levels indicate that the die geometry modified material shape, but did not induce enough plastic deformation to increase hardness. Moreover, roughness indicates a smaller real contact area and therefore during the straightening step was not possible to reach the baseline.

Table 2 summarizes root mean square roughness (Rrms) for baseline, deepest and highest zones, show-

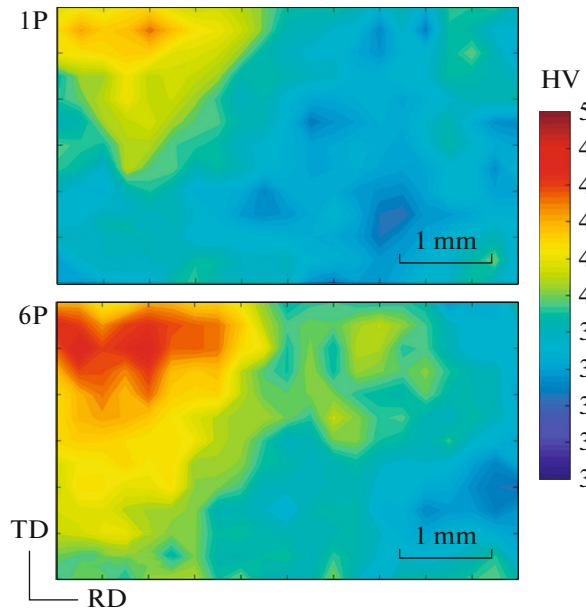


Fig. 3. Microhardness mapping for 1P and 6P samples.

ing a gradual increment in the last two, leading to 6P specimen to exhibited higher values, while in baseline levels Rrms are similar. This indicates that in the highest zones of both materials, a mild wear process reduces the Rrms values [32], in regard to baseline and deepest zones. A detailed overview of Fig. 4 and Table 2 allows to remark that main superficial effects of increasing the number of RCS passes were the increment in height gaps. However, under present conditions, substantial changes in roughness were produced only from 0P to 1P, while subsequent passes do not contribute to significant changes.

X-ray diffractograms in Fig. 5 show that 0P, 1P, 6P present a high relative intensity for (220) plane, this is particularly visible in 0P and indicates a preferred crystal orientation. Although 1P and 6P exhibit a relative increase of intensity for (111) and (200); predominant orientation still being (220), this behavior indicates that texture intensity variation along the process can be found between different RCS passes. A normalized peak broadening for (220) plane is shown in Fig. 6. Between 0P and 1P samples an increase in

Table 2. Rrms values for 0P, 1P, and 6P samples

RCS Pass	Rrms, μm baseline	Rrms, μm deepest zones	Rrms, μm highest zones
0P	0.56 ± 0.03		
1P	0.76 ± 0.12	0.87 ± 0.2	0.62 ± 0.7
6P	0.77 ± 0.18	0.92 ± 0.26	0.73 ± 0.13

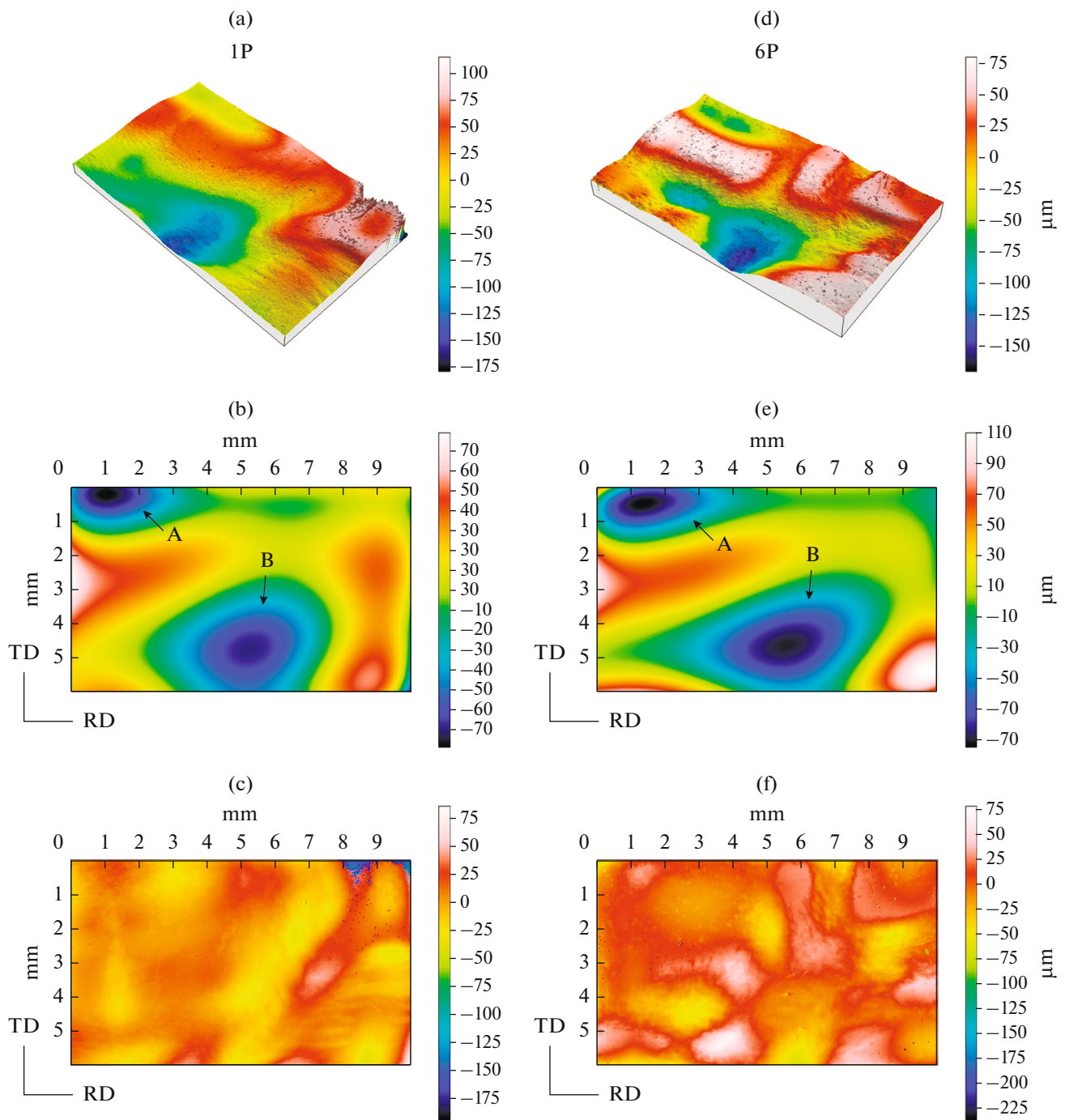


Fig. 4. (a) 3D height profile, (b) contours of shape and (c) roughness for 1P. (d) 3D height profile, (e) contours of the shape and (f) roughness for 6P.

FWHM was registered, this indicates a strain increase into the crystal or a decrease in grain size. In addition, between 1P and 6P there is a marginal decrement in peak broadening suggesting a dislocations rearrangement compatible with a partial stress release.

Based on the Le Bail XRD peaks profile matching, it is possible to understand the peak-broadening evolution during the RCS process. Figure 7 shows the

Williamson–Hall plots for several RCS passes. For 0P sample a negligible slope is observed; this indicates that as a consequence of the annealing treatment, the material underwent a stress relaxation associated with the lowest dislocation density. For 1P sample, the corresponding slope increase indicating the rise of dislocation density and probably the formation of some dislocation tangles. A slope reduction was observed

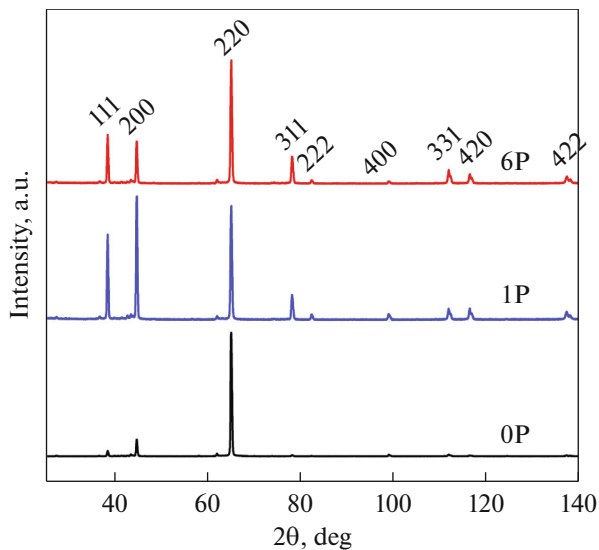


Fig. 5. X-ray diffractograms for 0P, 1P, and 6P samples.

between 1P and 4P and subsequently, no changes in slope were observed between 4P and 6P samples. The previous behavior has been observed in several works after SPD processing [33] and leads to one of two hypotheses; the first suggests the presence of several microcracks that generate a stress relaxation; the second indicates that at this stage, the material increased its capability of dislocation annihilation, even if it occurred during a cold work process [10, 14, 15, 34, 35]. Because no visible cracks were observed in the samples, the second hypothesis seems more probable. Moreover, β (y-intercept) values indicate an important reduction in crystallite domain after one RCS cycle, for 4P value remained unchanged and decreased again for 6P sample.

Figure 8, shows the texture evolution for 0P, 1P, and 6P samples. Main texture components and their respective volume fraction were computed by MTEX software. At annealing conditions, the two major components (P1 and P2) corresponding to annealed P orientation $\{100\}\langle 554 \rangle$ were found [36–38]. No change in texture components was observed for 1P, but its global intensity decreases, this could be related to substructure generation expected in early stages of SPD processes and agrees with X-ray peak-broadening results. In the case of 6P, the increasing spread some degrees around the original components, P1 and P2 was observed, this is caused by the specific RCS strain state which presumably activates different slip systems generating misorientation across subgrain boundaries and eventually promotes low angle grain boundaries (LAGB) and high angle grain boundaries (HAGB) [12]. Contrary to other SPD processes [33, 39–41], this RCS process applied to a 3003 AA sheet, did not modify the specific initial texture components, there-

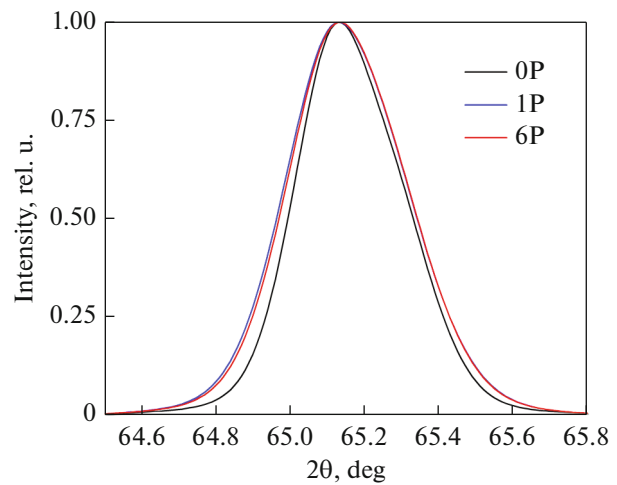


Fig. 6. (220) FWHM comparison for different samples.

fore, mechanical properties improvement is only related to dislocation density. Such behavior could be beneficial for industrial applications in which preserving the original grain orientation is often required.

Grain orientation maps obtained from EBSD (Fig. 9) showed that major structural modifications produced by plastic deformation consisted in substructure formation due to average grain size; previous works have shown that at the evaluated stage of the process, a condition of ultrafine grain has not been achieved [42]. However, comparing boundary misorientation angle histograms for 0P, 1P, and 6P, LAGB (5° – 15°) fraction increases as a function of RCS passes, having 7, 12, and 30%, respectively. Even if grain refinement has not begun, the LAGB fraction increase and Williamson–Hall plots indicate a sub-

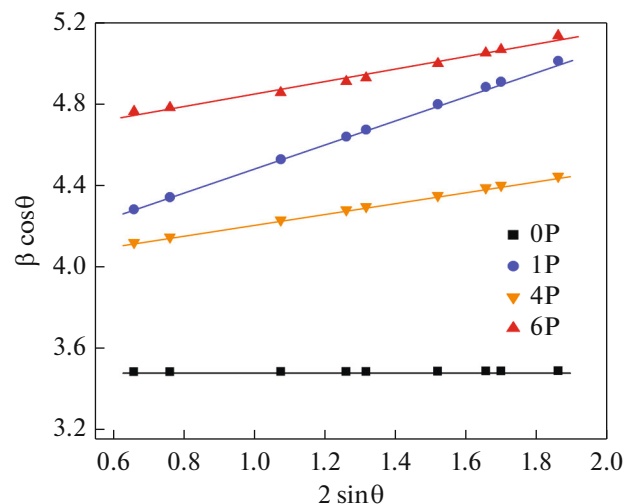


Fig. 7. W–H plots for samples at 0P, 1P, 4P, and 6P of RCS process.

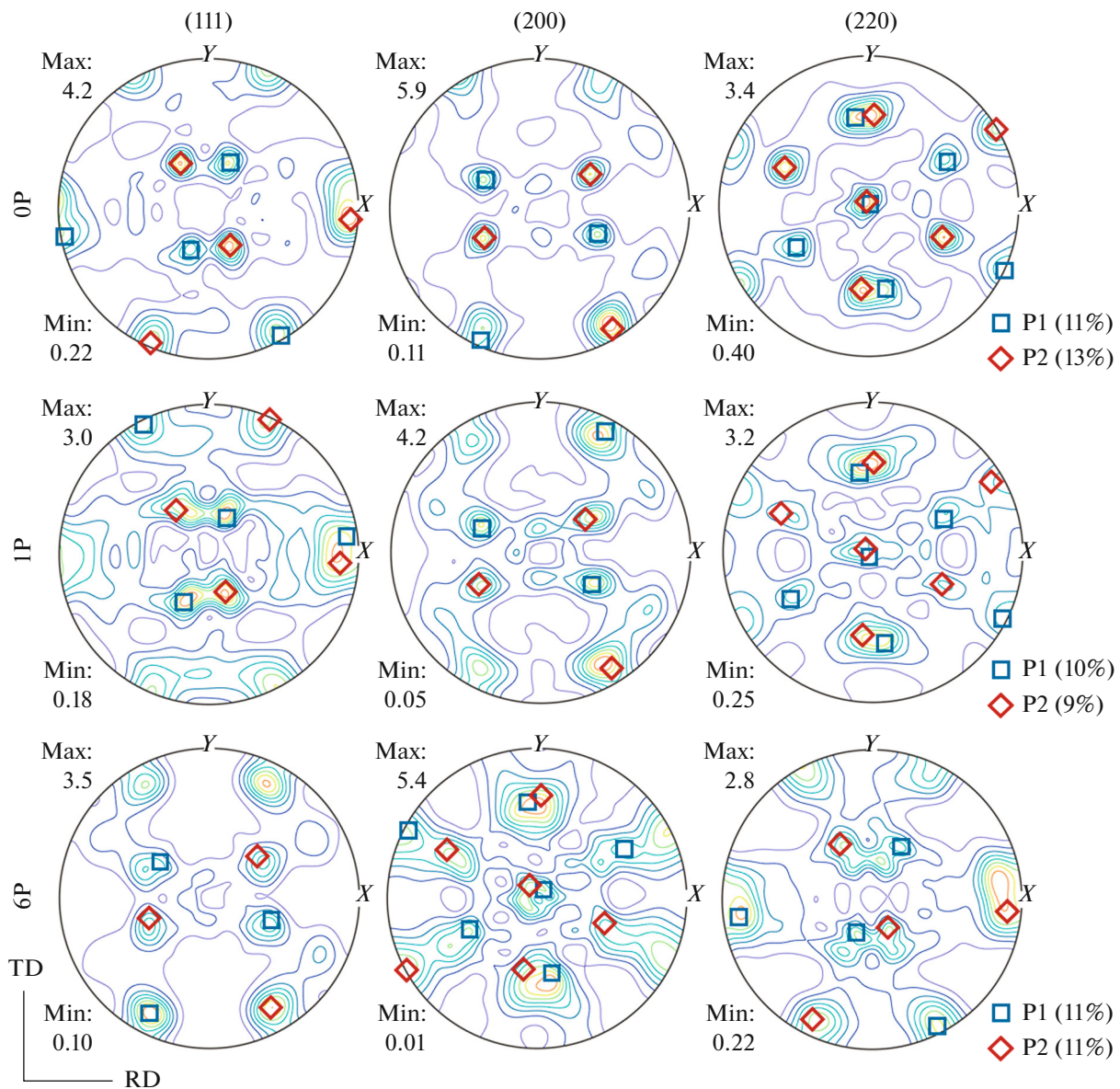


Fig. 8. Calculated pole figures with main texture components.

structure generation along the process, where dislocation density increased after one RCS cycle, decreases for 4P and remains still between 4P and 6P; plastic strain induced among those cycles generated dislocation density, however, dislocation rearrangement decreased crystallite domain, as well as internal deformation.

Local distribution of this LAGB fraction was corroborated by the computation of second order kernel average misorientation (KAM). KAM map presented in Fig. 10, which relates local misorientations with microhardness mapping, supporting that higher hardness values are corresponding to KAM increase, this corroborates that both characterization techniques

allow to determinate strain distribution induced by this particular RCS process.

Representative grains, which normal is parallel to $\langle 001 \rangle$, $\langle 011 \rangle$, and $\langle 111 \rangle$ were subjected to local misorientations evolution analysis. KAM histograms and their corresponding grain maps presented in Fig. 11 show that prior to RCS process (0P), grains have similar local misorientation independently of the normal directions. After the first RCS pass (1P), histograms show a shift to the right, which represents a general increment of local misorientations, indicating the beginning of grain fragmentation process that has a stronger effect over $\langle 111 \rangle$ grains. Further RCS passes (6P) maintain KAM displacement trend for $\langle 001 \rangle$ and $\langle 011 \rangle$ crystals, in contrast with $\langle 111 \rangle$ grains, which

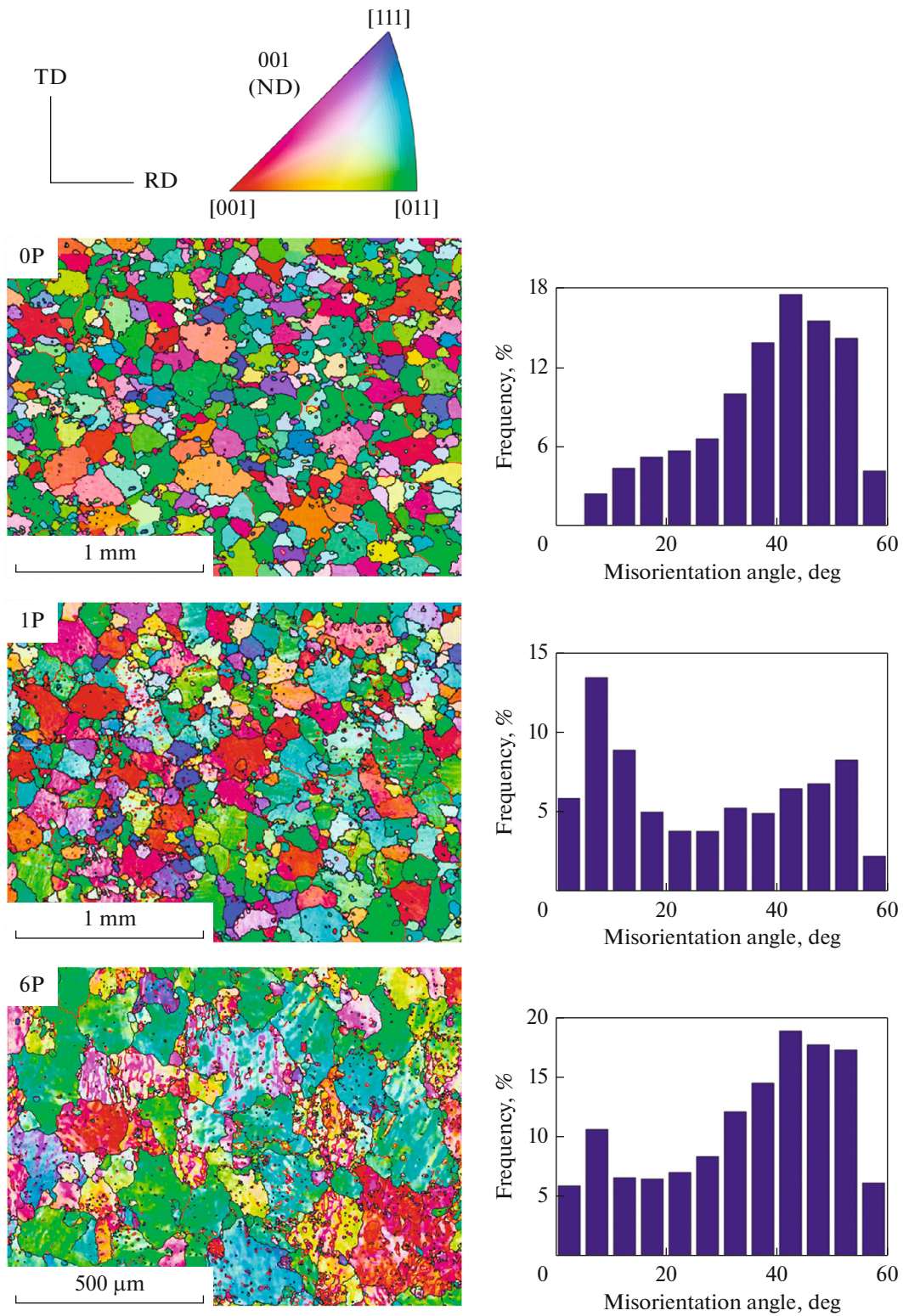


Fig. 9. Orientation maps and their corresponding grain boundary misorientation histograms for 0P, 1P, and 6P.

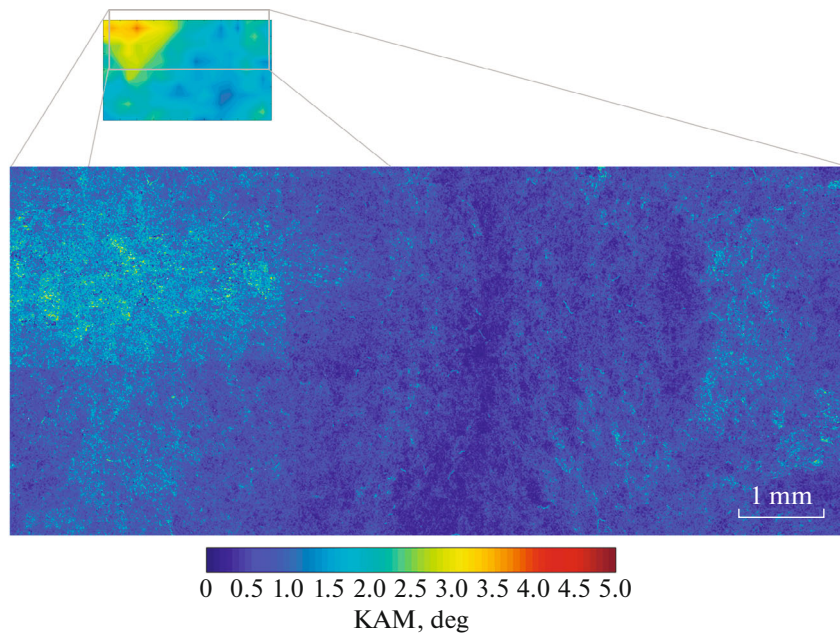


Fig. 10. KAM map for 1P showing the location of the measured region into the hardness mapping.

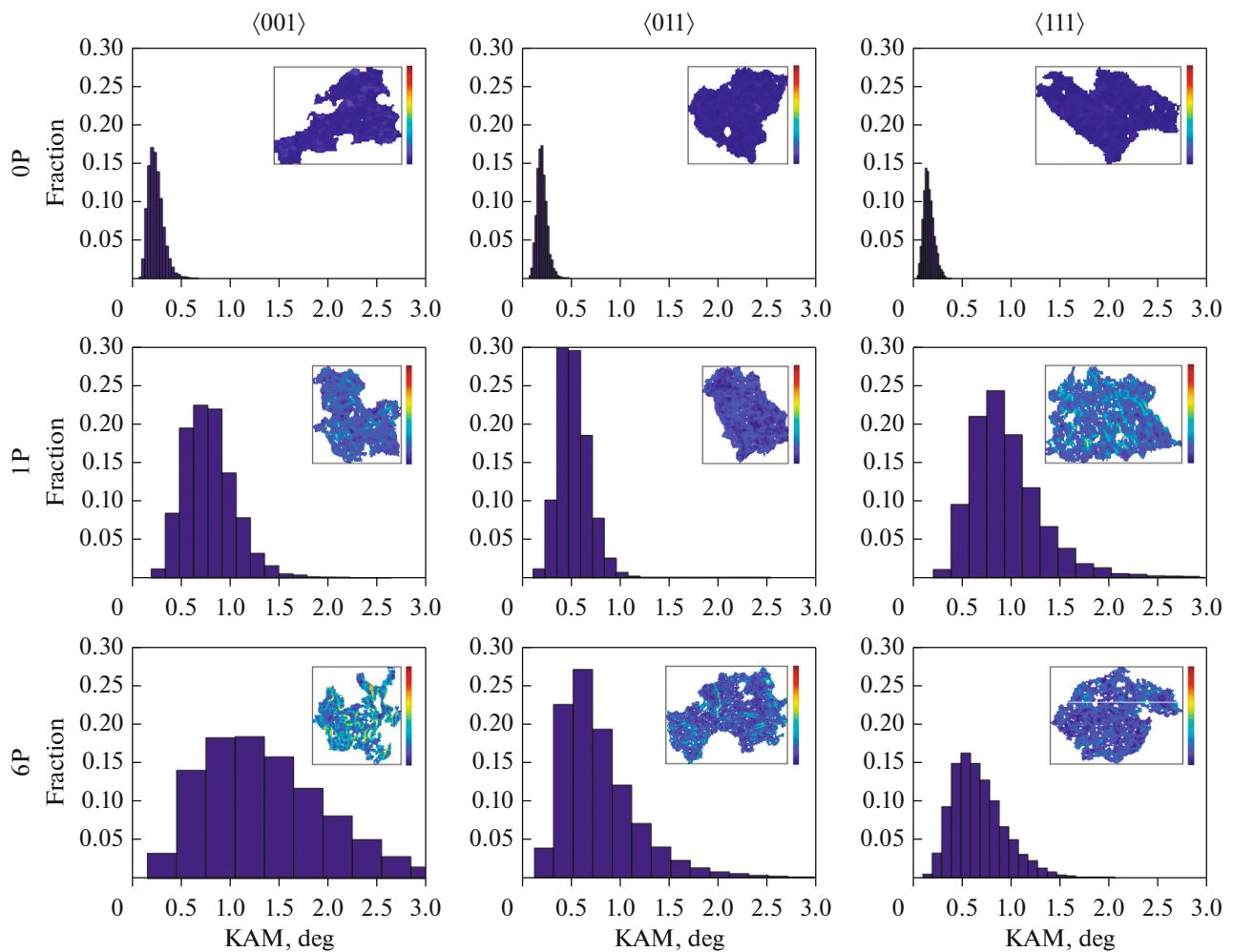


Fig. 11. KAM distribution histograms and their corresponding KAM maps of grain, which normal is parallel to $\langle 001 \rangle$, $\langle 011 \rangle$, and $\langle 111 \rangle$, for 0P, 1P, and 6P.

exhibited a shift to lower KAM values, indicating that the dislocation rearrangement process was activated prior to other directions grains. The latest matches with results showed above, where a decrease in W–H plot slope magnitude was registered for 6P specimen.

CONCLUSIONS

The novel die geometry proposed in the present study produced mechanical, superficial, and microstructural modifications that conduce to a general improvement in properties, allowing to expand the applications field of 3003 aluminum alloy sheets.

Yield strength was enhanced since early stages of the process. Heterogeneous strain distribution induced was determined by hardness mapping, showing that regions that presented higher hardness and larger contact area after one RCS pass expanded as the number of passes increases.

The analyzed RCS process did not change the initial texture components, this could be beneficial if the strength increase is required without changes in grain orientation. Also, RCS process introduced a large number of low angle grain boundaries, indicating that further RCS passes would lead to grain refinement.

It was determined that grains, which normal is parallel to $\langle 111 \rangle$ presented dislocation rearrangement and cells formation in early RCS stages prior to grains $\langle 001 \rangle$, $\langle 011 \rangle$. Furthermore, W–H plots are consistent with dislocation rearrangement of grains $\langle 111 \rangle$, which reduces local misorientation values.

ACKNOWLEDGMENTS

Reyes-Ruiz gratefully acknowledges to DGAPA for his postdoctoral fellowship. G. Gonzalez acknowledges the funding support by PAPIIT IN107917. Authors wish to thank technical support by E. Hernández-Mecinas, Adriana Tejada, and Omar Novelo.

REFERENCES

1. I. Sabirov, M. Y. Murashkin, and R. Z. Valiev, "Nanostructured aluminium alloys produced by severe plastic deformation: New horizons in development," *Mater. Sci. Eng., A* **560**, 1–24 (2013).
2. T. G. Langdon, "The processing of ultrafine-grained materials through the application of severe plastic deformation," *J. Mater. Sci.* **42**, 3388–3397 (2007).
3. R. Z. Valiev, M. Y. Murashkin, A. V. Ganeev, and N. A. Enikeev, "Superstrength of nanostructured metals and alloys produced by severe plastic deformation," *Phys. Met. Metallogr.* **113**, 1193–1201 (2012).
4. V. M. Segal, "Severe plastic deformation: simple shear versus pure shear," *Mater. Sci. Eng., A* **338**, 331–344 (2002).
5. Y. Iwahashi, J. Wang, Z. Horita, M. Nemoto, and T. G. Langdon, "Principle of equal-channel angular pressing for the processing of ultra-fine grained materials," *Scr. Mater.* **35**, 143–146 (1996).
6. R. Z. Valiev and T. G. Langdon, "Principles of equal-channel angular pressing as a processing tool for grain refinement," *Prog. Mater. Sci.* **51**, 881–981 (2006).
7. J. Zhang, N. Gao, and M. J. Starink, "Microstructure development and hardening during high pressure torsion of commercially pure aluminum: Strain reversal experiments and a dislocation based model," *Mater. Sci. Eng., A* **528**, 2581–2591 (2011).
8. G. Liu, J. Gu, S. Ni, Y. Liu, and M. Song, "Microstructural evolution of Cu–Al alloys subjected to multi-axial compression," *Mater. Charact.* **103**, 107–119 (2015).
9. K. Hajizadeh, S. Ejtemaei, B. Eghbali, and K. J. Kurzydowski, "Microstructure and mechanical properties of 1050 aluminum after the combined processes of constrained groove pressing and cold rolling," *Phys. Met. Metallogr.* **121**, 72–77 (2020).
10. A. A. Tohidi, M. Ketabchi, and A. Hasannia, "Nanograined Ti–Nb microalloy steel achieved by Accumulative Roll Bonding (ARB) process," *Mater. Sci. Eng., A* **577**, 43–47 (2013).
11. J. Huang, Y. T. Zhu, D. J. Alexander, X. Liao, T. C. Lowe, and R. J. Asaro, "Development of repetitive corrugation and straightening," *Mater. Sci. Eng., A* **371**, 35–39 (2004).
12. J. Y. Huang, Y. T. Zhu, H. Jiang, and T. C. Lowe, "Microstructures and dislocation configurations in nanostructured Cu processed by repetitive corrugation and straightening," *Acta Mater.* **49**, 1497–1505 (2001).
13. I. G. Brodova, E. V. Shorokhov, I. G. Shirinkina, I. N. Zhgilev, T. I. Yablonskikh, V. V. Astaf'ev, and O. V. Antonova, "Evolution of the structure formation during dynamic pressing of the AMts alloy," *Phys. Met. Metallogr.* **105**, 594–601 (2008).
14. R. Pippin, F. Wetscher, M. Hafok, A. Vorhauer, and I. Sabirov, "The limits of refinement by severe plastic deformation," *Adv. Eng. Mater.* **8**, 1046–1056 (2006).
15. I. E. Volokitina and A. V. Volokitin, "Evolution of the microstructure and mechanical properties of copper during the pressing–drawing process," *Phys. Met. Metallogr.* **119**, 917–921 (2018).
16. G. H. Zahid, Y. Huang, and P. B. Prangnell, "Microstructure and texture evolution during annealing a cryogenic-SPD processed Al-alloy with a nanoscale lamellar HAGB grain structure," *Acta Mater.* **57**, 3509–3521 (2009).
17. E. C. Moreno-Valle, I. Sabirov, M. T. Perez-Prado, M. Y. Murashkin, E. V. Bobruk, and R. Z. Valiev, "Effect of the grain refinement via severe plastic deformation on strength properties and deformation behavior of an Al6061 alloy at room and cryogenic temperatures," *Mater. Lett.* **65**, 2917–2919 (2011).
18. D. B. Witkin and E. J. Lavernia, "Synthesis and mechanical behavior of nanostructured materials via cryomilling," *Prog. Mater. Sci.* **51**, 1–60 (2006).
19. F. Khodabakhshi, M. Abbaszadeh, H. Eskandari, and S. R. Mohebpour, "Application of CGP-cross route process for microstructure refinement and mechanical properties improvement in steel sheets," *J. Manuf. Process.* **15**, 533–541 (2013).

20. H. Lianxi, L. Yuping, W. Erde, and Y. Yang, "Ultrafine grained structure and mechanical properties of a LY12 Al alloy prepared by repetitive upsetting-extrusion," *Mater. Sci. Eng., A* **422**, 327–332 (2006).
21. F. Khodabakhshi and A. P. Gerlich, "Accumulative fold-forging (AFF) as a novel severe plastic deformation process to fabricate a high strength ultra-fine grained layered aluminum alloy structure," *Mater. Charact.* **136**, 229–239 (2018).
22. A. Shokuhfar and O. Nejadseyfi, "A comparison of the effects of severe plastic deformation and heat treatment on the tensile properties and impact toughness of aluminum alloy 6061," *Mater. Sci. Eng., A* **594**, 140–148 (2014).
23. N. Thangapandian, S. B. Prabu, and K. A. Padmanabhan, "Effects of die profile on grain refinement in Al–Mg alloy processed by repetitive corrugation and straightening," *Mater. Sci. Eng., A* **649**, 229–238 (2016).
24. N. Thangapandian, S. B. Prabu, and K. A. Padmanabhan, "On the role of experimental variables in the repetitive corrugation and straightening of an Al–Mg alloy," *Procedia Eng.* **207**, 1457–1462 (2017).
25. X. Wu and Y. Zhu, "Heterogeneous materials: a new class of materials with unprecedented mechanical properties," *Mater. Res. Lett.* **5**, 527–532 (2017).
26. A. Rosochowski, "Processing metals by severe plastic deformation," *Solid State Phenom.* **101–102**, 13–22 (2005).
27. F. Bachmann, R. Hielscher, and H. Schaeben, "Texture analysis with MTEX – free and open source software toolbox," *Solid State Phenom.* **160**, 63–68 (2010).
28. T. Roisnel and J. Rodríguez-Carvajal, "WinPLOTR: A windows tool for powder diffraction pattern analysis," *Mater. Sci. Forum* **378–381**, 118–123 (2001).
29. S. S. Satheesh Kumar and T. Raghu, "Structural and mechanical behaviour of severe plastically deformed high purity aluminium sheets processed by constrained groove pressing technique," *Mater. Des.* **57**, 114–120 (2014).
30. Y. Estrin and A. Vinogradov, "Extreme grain refinement by severe plastic deformation: A wealth of challenging science," *Acta Mater.* **61**, 782–817 (2013).
31. C. Figueroa, R. Schouwenaars, V. Jacobo, A. Ortiz, R. Petrov, and L. Kestens, "Tribological and microstructural characterization of ultrafine layers induced by wear in ductile alloys," *Tribol. Online.* **11**, 389–395 (2016).
32. J. Williams, *Engineering Tribology* (Cambridge University, Cambridge, 2005).
33. C. Reyes-Ruiz, I. A. Figueroa, C. Braham, J. M. Cabrera, I. Alfonso, and G. Gonzalez, "Texture and lattice distortion study of an Al-6061-T6 alloy produced by ECAP," *Mater. Trans.* **56**, 1781–1786 (2015).
34. W. Skrotzki, A. Eschke, B. Joni, T. Ungar, L. S. Toth, Y. Ivanisenko, and L. Kurmanaeva, "New experimental insight into the mechanisms of nanoplasticity," *Acta Mater.* **61**, 7271–7284 (2013).
35. O. Renk, A. Hohenwarter, S. Wurster, and R. Pippan, "Direct evidence for grain boundary motion as the dominant restoration mechanism in the steady-state regime of extremely cold-rolled copper," *Acta Mater.* **77**, 401–410 (2014).
36. J. Liu and J. G. Morris, "Recrystallization Textures of continuous cast AA 3015 alloy: Development of the P orientation {011} (566)," *Metall. Mater. Trans. A* **34**, 2029–2032 (2003).
37. W. X. Wang, M. Ma, H. L. Li, J. X. Zhang, and W. C. Liu, "Effect of preheat treatment on the texture evolution during cold rolling of AA 3003 aluminum alloy," *J. Mater. Eng. Perform.* **24**, 4283–4289 (2015).
38. W. X. Wang, J. X. Zhang, Z. J. Wang, and W. C. Liu, "A comparative study of the transformation kinetics of recrystallization texture of CC and DC 3003 aluminum alloys," *Mater. Charact.* **141**, 412–422 (2018).
39. I. J. Beyerlein and L. S. Tóth, "Texture evolution in equal-channel angular extrusion," *Prog. Mater. Sci.* **54**, 427–510 (2009).
40. L. S. Tóth, "Texture evolution in severe plastic deformation by equal channel angular extrusion," *Adv. Eng. Mater.* **5**, 308–316 (2003).
41. C. G. Figueroa, R. Schouwenaars, J. Cortés-Pérez, R. Petrov, and L. Kestens, "Ultrafine gradient microstructure induced by severe plastic deformation under sliding contact conditions in copper," *Mater. Charact.* **138**, 263–273 (2018).
42. J. Jenix Rino, S. Balasivanandha Prabu, and K. A. Padmanabhan, "On the influence of repetitive corrugation and straightening on the microstructure and mechanical properties of AA 8090 Al–Li alloy," *Arch. Civ. Mech. Eng.* **18**, 280–290 (2018).